






Article

Investigation of High-Efficiency and Stable Carbon-Perovskite/Silicon and Carbon-Perovskite/CIGS-GeTe Tandem Solar Cells

Ahmed Saeed ¹, Mostafa M. Salah ^{1,*}, Abdelhalim Zekry ², Mohamed Mousa ¹, Ahmed Shaker ², Mohamed Abouelatta ², Fathy Z. Amer ³, Roaa I. Mubarak ³ and Dalia S. Louis ²

¹ Electrical Engineering Department, Future University in Egypt, Cairo 11835, Egypt

² Faculty of Engineering, Ain Shams University, Cairo 11535, Egypt

³ Electronics & Communication Engineering Department, Faculty of Engineering, Helwan University, Cairo 11795, Egypt

* Correspondence: mostafa.abdulkhalek@fue.edu.eg

Abstract: The primary purpose of recent research on solar cells is to achieve a higher power conversion efficiency with stable characteristics. To push the developments of photovoltaic (PV) technology, tandem solar cells are being intensively researched, as they have higher power conversion efficiency (PCE) than single-junction cells. Perovskite solar cells (PSCs) are recently used as a top cell of tandem solar cells thanks to their tunable energy gap, high short circuit current, and low cost of fabrication. One of the main challenges in PSCs is the stability issue. Carbon perovskite solar cells (CPSCs) without a hole transport material (HTM) presented a promising solution for PSCs' stability. The two-terminal monolithic tandem solar cells demonstrate the commercial tandem cells market. Consequently, all the proposed tandem solar cells in this paper are equivalent to two-terminal monolithic tandem devices. In this work, two two-terminal tandem solar cells are proposed and investigated using the SCAPS-1D device simulator. Carbon perovskite solar cell (CPSC) without hole transport material (HTM) is used as the top cell with a new proposed gradient doping in the perovskite layer. This proposal has led to a substantial enhancement of the stability issue known to be present in carbon perovskite cells. Moreover, a higher PCE, exceeding 22%, has been attained for the proposed CPSC. Two bottom cells are examined, Si and CIGS-GeTe solar cells. The suggested CPSC/Si and CPSC/CIGS-GeTe tandem solar cells have the advantage of having just two junctions, which reduces the complexity and cost of solar cells. The performance parameters are found to be improved. In specific, the PCEs of the two proposed cells are 19.89% and 24.69%, respectively.

Keywords: carbon perovskite solar cell (CPSC); copper indium gallium sulfide (CIGS); double absorbers; germanium telluride (GeTe); high voltage; SCAPS-1D; zinc selenide (ZnSe)



Citation: Saeed, A.; Salah, M.M.; Zekry, A.; Mousa, M.; Shaker, A.; Abouelatta, M.; Amer, F.Z.; Mubarak, R.I.; Louis, D.S. Investigation of High-Efficiency and Stable Carbon-Perovskite/Silicon and Carbon-Perovskite/CIGS-GeTe Tandem Solar Cells. *Energies* **2023**, *16*, 1676. <https://doi.org/10.3390/en16041676>

Academic Editor: Peter D. Lund

Received: 4 January 2023

Revised: 29 January 2023

Accepted: 1 February 2023

Published: 8 February 2023



Copyright: © 2023 by the authors. Licensee MDPI, Basel, Switzerland. This article is an open access article distributed under the terms and conditions of the Creative Commons Attribution (CC BY) license (<https://creativecommons.org/licenses/by/4.0/>).

1. Introduction

Recently, significant growth in energy demand, which strongly required changing conventional energy resources to green resources, has been reported. This transition is restricted by several important factors among which is the increase in gadget dependability [1]. PV technology appears to be a potential solution that produces clean energy [2]. Nowadays, the PV market is led by silicon-based technology where silicon-based cells have PCEs that exceed 25% [2]. Thin film PVs, like dye-sensitized, CIGS, and PSCs, have low-cost fabrication processes and contain various semiconductor materials, which can be deposited on different substrates.

PSCs have simple fabrication techniques and great performance, allowing them to be widely investigated and used [3]. Moreover, they have a tunable energy gap, high short circuit current (J_{sc}), long diffusion lengths, and low recombination rates. Consequently, these cells can be considered good candidates for conventional solar cells. Recently, PSCs

with PCEs up to 25% have been reported [4]. Because of these characteristics, PSCs are excellent candidates for traditional solar cells. The perovskite substance has the composition ABX_3 . A is organic ammonium, such as MA, and B is a metal cation, (e.g., Pb^{2+}). X is a halide anion (e.g., I, Br, Cl). In the crystal structure, the A ion is surrounded by eight three-dimensional structures of corner-sharing octahedral BX_6 units [5]. This structure is the composition of calcium titanium oxide ($CaTiO_3$), which was found in 1839 [6]. The first photocurrent of barium titanium oxide ($BaTiO_3$) was observed in 1956 [7]. From 2009 to 2016, PSCs manufactured from hybrid-halide materials of methylammonium lead-halides ($CH_3NH_3PbX_3 = MAPbX_3$) by various designs, showed enhanced PCEs around 25% [8]. The development of PSC in recent years has produced simulation results of up to more than 30% [9].

The traditional structure of the PSCs is the electron transport material (ETM)/perovskite/HTM [10]. However, one of the critical problems is that conventional organic HTMs are often expensive and unstable [11], which is one of the addressed problems in this paper. Additionally, noble metal electrodes are likewise quite pricey [12]. It was noticed that PSCs without HTMs might also work well since the unique conductivity feature of the perovskite material allows it to function not only as absorbers but also as HTMs [13]. CPSCs without HTM show great potential for resolving the concerns mentioned above [14]. Carbon materials are abundant on the earth, low-cost, and stable [15]. The first CPSCs were published in 2013 and had a record PCE of $\approx 6.6\%$ [16]. In 2014, a CPSC was reported with long-term stability and the highest PCE of 12.8% until 2016 [17]. In 2016, by using a solvent engineering technique to monitor thermodynamics and conversion kinetics, a pure perovskite was fabricated. The carbon/perovskite interface was enhanced by preparing low defects absorber, and the PCE exceeded 14% [18]. In 2018, all introduced CPSCs had a PCE that exceeded 15% [19]. Although significant improvements in CPSCs over the last few years were encountered, the maximum recorded PCE of CPSCs was around 16% [20,21].

On the other hand, given that CIGS solar cells have a small share of the PV market, it was appealing to examine this potential material for usage with other absorbers to offer a competitive advantage over other alternatives. Also, GeTe is another interesting material since its energy gap is 0.8 eV, and its absorption coefficient exceeds $2.7 \times 10^4 \text{ cm}^{-1}$. It is expected that this promising material will be employed as an absorber for solar cells due to its encouraging optoelectronic properties. In this paper, besides Si, CIGS and GeTe are utilized as double absorbers back-cell of the simulated tandem solar cells.

The PCEs of single-junction cells are remarkably restricted since the absorbed photons are only those having energies equal to or larger than the energy gap of the employed absorbers [22]. It has been reported theoretically that the PCE_{max} of single-junction solar cells is 33.7% for absorbers with an energy gap of 1.34 eV [23]. The limitation of this PCE can be surpassed by multi-junction (tandem) solar cells. Using different absorbers in an infinite number of sub-cells to construct a tandem solar cell, has shown theoretically an increased PCE to 68.2% [24]. In this case, the cell with the highest absorber energy gap is used as the front cell, and the one with the lowest energy gap is the bottom cell [25]. The most widely used tandem solar cell is the monolithic two-terminal type since it has the lowest fabrication cost, as it uses the minimum number of transparent conducting oxide (TCO). The main problem of this kind of tandem is the current matching of all the sub-cells. In this paper, an optimization algorithm is employed to determine the thickness of the absorber of the top cell.

Based on the previous discussion, CPSC is proposed as a top cell of the suggested two-terminal tandem solar cells to provide a technique to alleviate the instability issue in conventional PSCs. Although PSC/Si tandem solar cells may be a good choice due to the availability of materials used, the high cost of fabrication can restrict the commercial spread of these cells. Consequently, CPSC/CIGS-GeTe tandem solar cell is also proposed to offer higher PCE with low-cost fabrication.

The rest of this article is structured as follows; the structure and materials of the suggested solar cells are described in Section 2. In Section 3, the results of the CPSC/Si and

CPSC/CIGS-GeTe tandem solar cells are discussed; and lastly, the conclusion is presented in Section 4.

2. Materials and Methods

SCAPS-1D is a useful program to design and study various types of SCs, which has been widely verified vs experimental solar cells [26]. It can simulate solar cells with up to seven layers. Most materials parameters can be assigned such as thickness, energy gap, affinity, permittivity, mobility, and concentration of doping and other physical or geometrical parameters [27–29].

The numerical solution in SCAPS-1D solves the basic physical differential equations in a steady state. The main equations are the continuity equations and Poisson's equation, which are solved self-consistently until convergence occurs. Firstly, the cell geometry is inserted. Then, the materials parameters are defined [30]. Poisson's equation and continuity equations are discretized into different mesh points. Discretization is executed by implying the finite difference method (FEM), and the current densities are modeled using the Scharfetter–Gummel process [31]. In the assigned mesh points, ψ , n , and p are iteratively computed by the Gummel method [32]. Physical models such as G , U , μ_n , and μ_p are enhanced after each iteration. Finally, we can obtain J - V , C - V , C - F , QE , AC , G , U , and energy diagrams [33].

In this work, two distinct two-terminal tandem solar cells are suggested. CPSC is considered the top cell of the suggested tandem solar cells while Si cell and CIGS-GeTe double absorber cell are used as the bottom cells to provide a comparative study between the two types and to draw some recommendations about the most suitable path. Figure 1a,b) illustrates the two proposed structures of the tandem solar cells, namely Si and CIGS-GeTe bottom cells, respectively. The CPSC structure is composed of fluorine-doped tin oxide (FTO) (4.6 eV) as the TCO, Zinc Selenide (ZnSe) as ETM, two perovskite layers with gradient doping as a concurrent absorber and HTM, and Carbon (5 eV) as back contact. The bottom cells consist of ZnO and CdS as n-type windows, while Si and CIGS-GeTe are used as p-type absorber materials. The front cell is illuminated by AM1.5G irradiance, while the incident spectrum to the rear cell is filtered AM1.5G after the front cell absorption. Filtered AM1.5G is given by Equation (1) [34], while the absorption coefficient (α) is given by Equation (2) [35].

$$S(\lambda) = S_o(\lambda) \cdot \prod_{x=1}^n e^{-\alpha_x d_x} \quad (1)$$

$$\alpha(E) = A_\alpha \sqrt{h\nu - E_g} \quad (2)$$

Table 1 presents the parameters employed in the mentioned equations as well as their definitions. All simulations are performed by the SCAPS-1D device simulator [36] which is widely used in simulating single-junction and tandem solar cells. A variety of photoactive absorbers have been implemented employing this software package. In addition, numerous studies have been performed and validated against practical work [9,25,30,37].

Table 1. Key incident and transmitted spectrum parameters.

Symbol	Definition	Unit
$S(\lambda)$	The power density of the spectrum transferred from the front sub-cell to the rear sub-cell	W/m ²
$S_o(\lambda)$	The incident irradiance is AM 1.5G	
x	Layer number	
n	The overall number of layers in a sub-cell	cm ^{−1}
α	The absorption coefficient of the material	
d	The layer thickness	cm
A_α	A pre-factor of 10 ⁵	cm ^{−1} .eV ^{−1/2}
h	Planck's constant	eV.sec
ν	Frequency	Hz
E_g	The energy gap of the material	eV

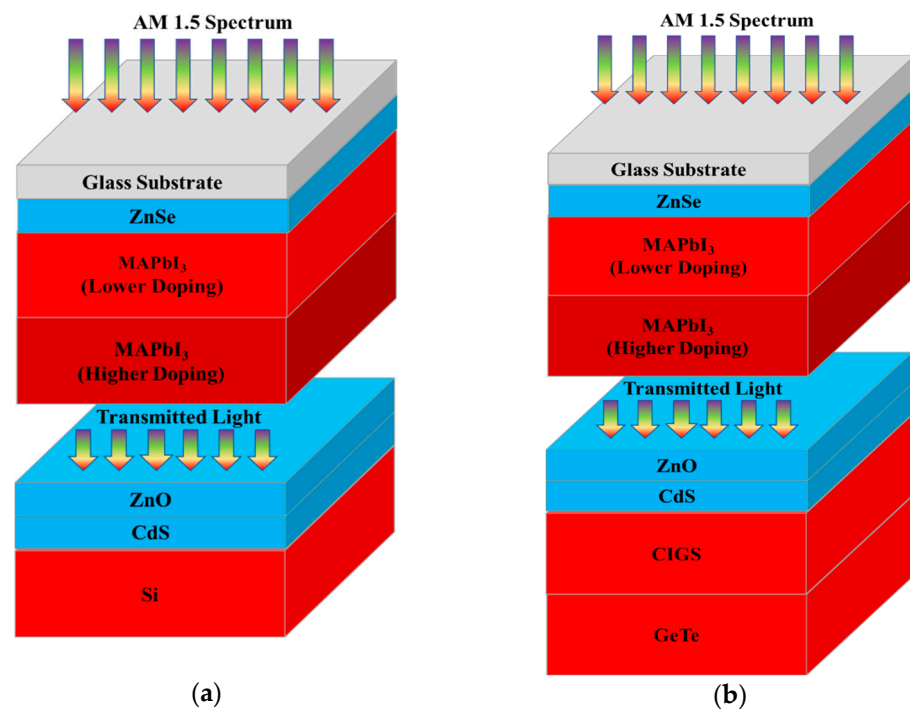


Figure 1. Illustration of structures of the proposed tandem solar cells (a) CPSC/Si, and (b) CPSC/CIGS-GeTe.

2.1. The Top Cell

The CPSC structure is investigated and simulated using SCAPS-1D. The resulting simulations have been validated and compared to published practical work [18]. The structure of this work is FTO, titanium dioxide (TiO_2) as ETM, MAPbI_3 , and Carbon as a back contact, respectively [18]. The main material parameters are recorded in Table 2 which are extracted from the appropriate literature. Figure 2 compares the experimental and simulation of the current-voltage (JV) and external quantum efficiency (EQE) curves. The key metrics of the simulation are in decent agreement with those experimentally reported. The performance factors of the experimental and calibrated CPSCs are presented in Table 3.

Table 2. Material parameters of the proposed tandem solar cells.

Parameters	Si	CIGS	GeTe [38]	MAPbI_3	TiO_2	CdS	ZnSe	ZnO [39]
Thickness (nm)	2000	2000–3000	2000	Variable	400	400	400	400
E_g (eV)	1.12	1.04–1.67 [40]	0.8	1.5–1.63 [41,42]	3.2 [43]	2.4 [44]	2.81 [45]	3.3
χ (eV)	4.05	4.5	4.8	3.9 [35]	4.1 [18]	4.18 [44]	4.09 [46]	4
ϵ_r	11.9	13.6 [47]	36	6.5 [48]	9 [49]	10 [44]	8.6 [50]	9
N_c (cm^{-3})	2.8×10^{19}	2.2×10^{18}	10^{16}		2.2×10^{18} [37,48,51]			
N_v (cm^{-3})	2.65×10^{19}	1.8×10^{19}	10^{17}	1.8×10^{19} [48]	1.8×10^{19} [37]		1.8×10^{19} [51]	
$v_{th,n}, v_{th,p}$ (cm/s)				1×10^7 [4]				
μ_e ($\text{cm}^2 \text{V}^{-1} \text{s}^{-1}$)	1450	100	100	2 [48]		100 [44]	400 [52]	100
μ_p ($\text{cm}^2 \text{V}^{-1} \text{s}^{-1}$)	500	25	20	2 [48]	1 [53]	25 [44]	110 [52]	25
N_A (cm^{-3})		2×10^{16}		10^{16} – 10^{19}		0		
N_D (cm^{-3})			0			1×10^{18}		
N_t (cm^{-3})			10^{14}			2×10^{15}		

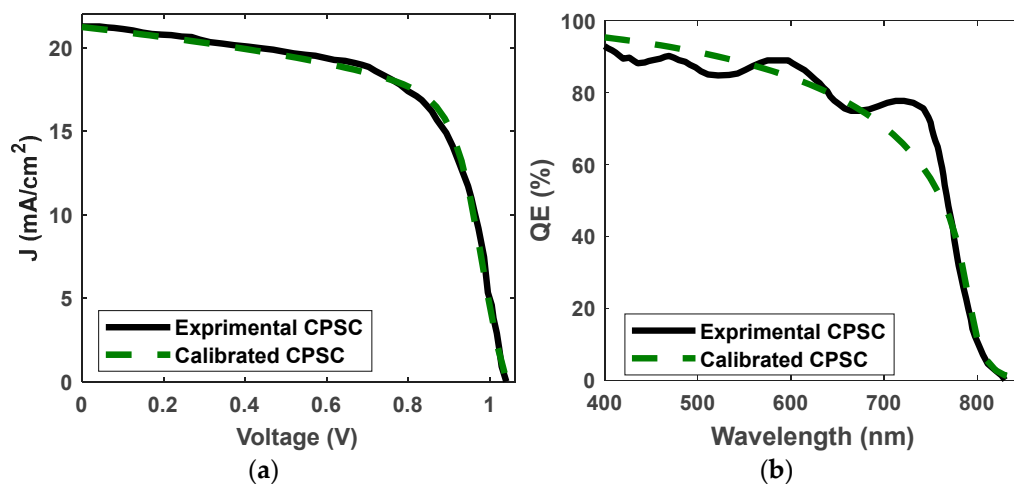


Figure 2. Validation of the simulated CPSC performance (a) JV curves and (b) EQE curves [18].

Table 3. Performance comparison of the experimental and calibrated CPSCs [18].

	V_{oc} (V)	J_{sc} (mA/cm ²)	FF (%)	PCE (%)
Experimental results	1.040	21.27	65.00	14.38
Simulation	1.041	21.23	65.01	14.38

Though significant improvements in CPSCs over the last few years were encountered, the maximum recorded PCE of CPSCs is still around 16% [21]. As can be deduced from the previous results, the performance is lower than the performance of PSCs with HTM. Splitting the absorber layer into two layers with different doping can generate an additional electric field that enhances the carriers' extraction. This approach has been applied to CZTS and silicon solar cells [54,55] and has been simulated for CPSC [56]. In this work, N_A of $1 \times 10^{17} \text{ cm}^{-3}$ is used for the low-doped perovskite film and $1 \times 10^{19} \text{ cm}^{-3}$ for the high-doped perovskite film, as displayed in Figure 1. The thickness of the ZnSe layer is 30 nm, and an N_D of $1 \times 10^{19} \text{ cm}^{-3}$. Here we employ ZnSe as a proposed ETM instead of the traditional ETMs since it has higher mobility and a narrower band gap. Implementing these modifications has led to a short circuit current density (J_{sc}) of 24.59 mA/cm², an open-circuit voltage (V_{oc}) of 1.19 V, FF of 76.08%, and PCE of 22.22%, as deduced from Figure 3a.

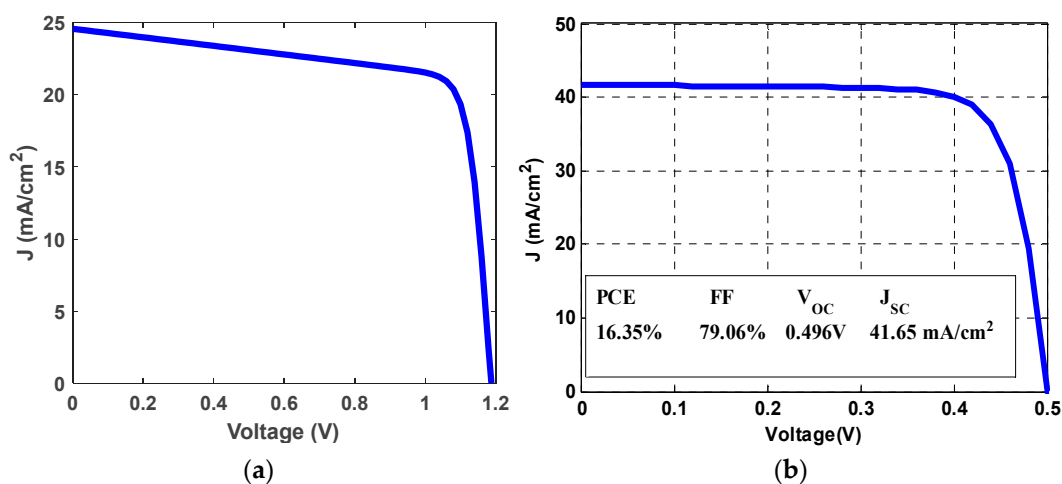


Figure 3. JV curves of (a) the modified CPSC, and (b) the Si solar cell and its outputs.

2.2. The Bottom Cells

The Si cell architecture is illustrated in Figure 1a. The simulated JV curve of the Si cell is illustrated in Figure 3b, with AM1.5G incident spectrum at 300 K temperature and the other simulation settings are the same as in the previous simulations. The simulation shows PCE = 16.35 % with FF = 79.06%, $V_{oc} = 0.496$ V and $J_{sc} = 41.65$ mA/cm². The output cell results are in good agreement with the state-of-the-art thin film Silicon-based solar cells [57].

A potential method to enhance the tandem solar cell efficiency can be accomplished by improving V_{oc} via increasing the doping level. Germanium Telluride (GeTe) can be heavily doped to increase the V_{oc} . However, this technique limits the current because increasing the doping results in deteriorating the minority lifetime, which consequently decreases the diffusion length. This can be explained based on Equations (3) to (7) [58–61]. In the mentioned equations, G is the generation rate, while L_p and L_n are the hole and electron diffusion lengths, respectively. The diffusion constant and the lifetime of the photoexcited carriers are denoted by D and τ , respectively.

$$J_{sc} = qG(L_n + L_p) \quad (3)$$

$$L_n = \sqrt{D\tau_n} \quad (4)$$

$$L_p = \sqrt{D\tau_p} \quad (5)$$

$$\tau_n \approx \frac{1}{C_n N_A^2} \quad (6)$$

$$\tau_p \approx \frac{1}{C_p N_D^2} \quad (7)$$

As can be inferred from the simple mathematical equations, high doping is responsible for a huge reduction in the current density and accordingly the PCE. A proposed solution is to reduce the GeTe layer thickness and add a Copper indium gallium selenide (CIGS) layer with a smaller thickness just above the GeTe thin film. This technique facilitates an increase in current flow and the bottom cell voltage as it serves as a series connection. The drawback of this structure is that the obtained cell current density is limited to the lowest current produced by the utilized absorbers.

Even though the small energy gap of GeTe declines V_{OC} , GeTe material can be more highly doped than CIGS, where the optimum doping concentration of the GeTe is in the order of 10^{20} [62]. So, an improvement will result as qV_{OC} depends on the energy variance of the acceptor material LUMO (E_{LUMO}^A) and the donor material HOMO (E_{HOMO}^D) which increases by doping. The V_{oc} can be written as in Equation (8) [63],

$$qV_{OC} = E_{LUMO}^A - E_{HOMO}^D - \Delta E_{loss} = E_{DA} - \Delta E_{loss} \quad (8)$$

where E_{DA} is the donor-acceptor effective energy gap. The energy loss that may occur when carriers are transferred to electrodes is denoted by ΔE_{loss} . This energy may be caused by many sources like Coulombic interactions and bimolecular recombination [64]. Equation (8) can be also written as (9),

$$qV_{OC} = E_{DA} - k_B T \ln(N_C N_V) + 2k_B T \ln \sqrt{np} \quad (9)$$

where n and p are the electron and hole density, respectively, T is the absolute temperature and k_B is the Boltzmann constant. N_V and N_C are effective densities of states for the HOMO and LUMO of the donors and acceptors' materials. As can be deduced from Equation (9), the voltage loss can be reduced by raising the doping density of the GeTe film. This ultimately increases the V_{OC} of the CIGS-GeTe sub-cell, because of increasing acceptor doping [63].

Now, the primary performance factors of the presented CIGS-GeTe sub-cell with various CIGS thicknesses ranging up to 1500 nm by a step of 500 nm are demonstrated in

Figure 4. The simulation results indicate that the maximum PCE occurs when the thickness of CIGS is 500 nm. Additionally, at these thicknesses, an appropriate J_{SC} is achieved. The CIGS-GeTe cell V_{OC} is higher than both CIGS and GeTe sub-cells. This can be explained as GeTe has a narrow energy gap, making it more absorbent at longer wavelengths. As illustrated in Figure 5a, the simulated JV curve of a CIGS-GeTe cell with an incident spectrum of AM1.5G has a V_{OC} of 0.784 V, a J_{SC} of 42.27 mA/cm², a PCE of 27.5 %, and an FF of 82.96%. Figure 5b illustrates the EQE of the suggested cell, signifying the good absorption in longer wavelengths up to about 1150 nm.

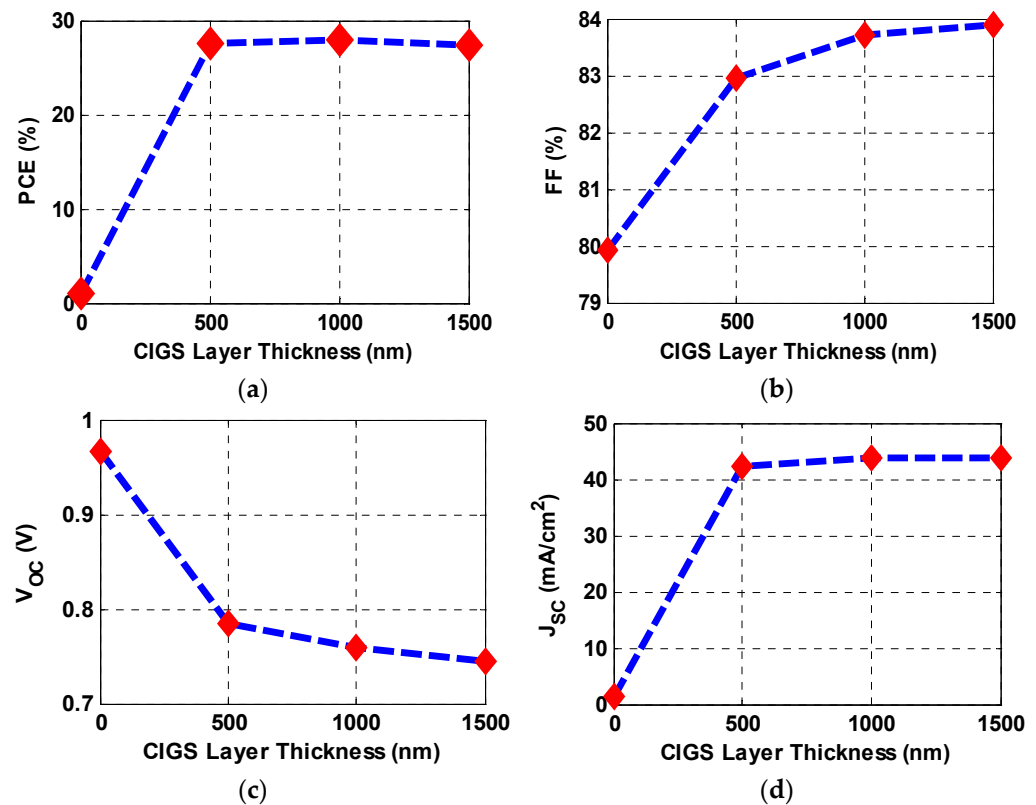


Figure 4. Effect of CIGS film thickness for the CIGS-GeTe absorber: (a) PCE, (b) FF, (c) V_{OC} , and (d) J_{SC} .

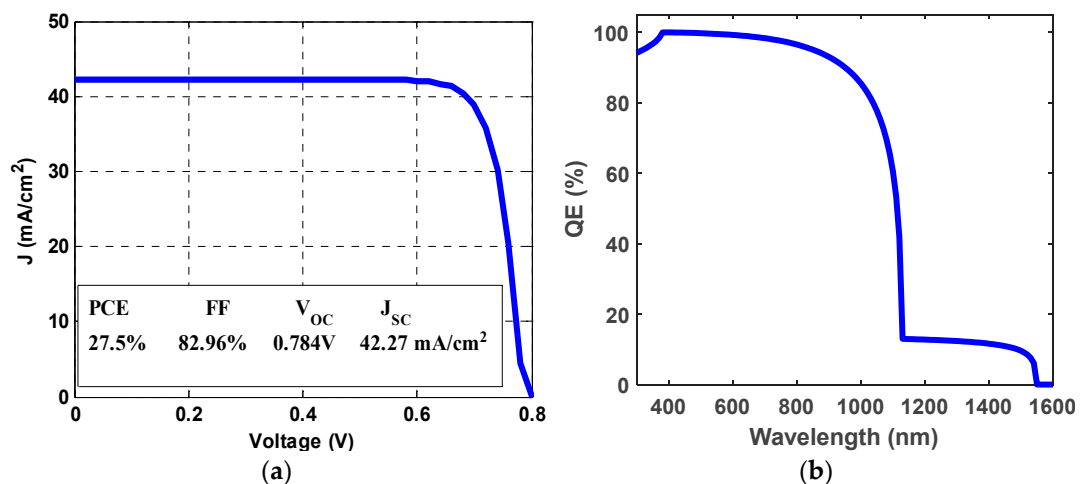


Figure 5. (a) CIGS-GeTe solar cell outputs and its JV curve and (b) EQE curve.

3. Results and Discussion

3.1. CPSC/Si Tandem Solar Cell

The CPSC/Si tandem solar cell was analyzed when the top cell photoactive layer thickness is varied by using the optimization algorithm explained in [22] as revealed in Figure 6a. The cell output factors of the tandem at 250 nm are PCE of 19.89%, FF of 85.1%, V_{OC} of 1.66 V, and J_{SC} of 14.08 mA/cm^2 , as the JV curve is shown in Figure 6b. The EQEs of the top, bottom, and tandem are given in Figure 7a. Figure 7b illustrates the absorbed spectrum of AM1.5G by the CPSC/Si tandem solar cell. The cut-off wavelength of this tandem solar cell is about 1120 nm according to the energy gap of the silicon.

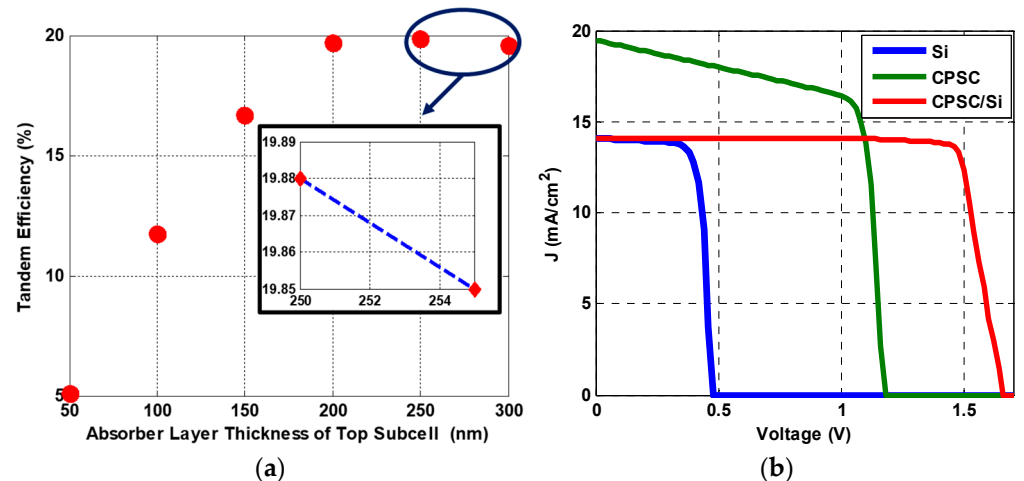


Figure 6. (a) PCE of CPSC/Si tandem solar cell with top cell absorber layer's thickness, and (b) JV characteristics of CPSC/Si sub-cells along with the tandem solar cell.

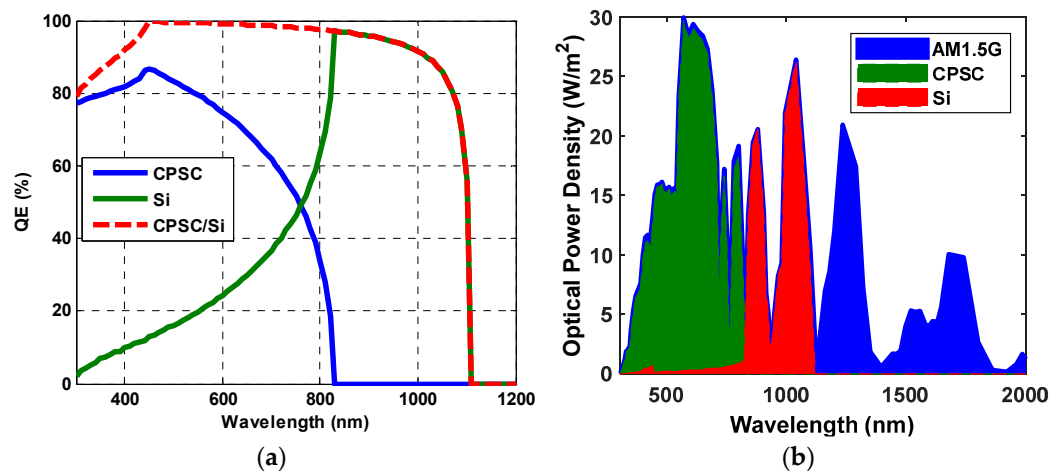


Figure 7. (a) EQE curves of CPSC/Si sub-cells and tandem solar cell, and (b) the absorbed spectrum of AM1.5G by the CPSC/Si tandem solar cell.

3.2. CPSC/CIGS-GeTe Tandem Solar Cell

Figure 8a shows the PCE variation of the CPSC/CIGS-GeTe tandem solar cell with the front cell absorber film thickness. The results reveal that at 255 nm top cell absorber thickness, the tandem solar cell can achieve the highest PCE of 24.69%. In Figure 8b, the JV curves of the top, bottom, and tandem are presented. V_{OC} of the tandem solar cell is 1.92 V, J_{SC} is 14.74 mA/cm^2 , and FF is 87.24%. Figure 9a shows the QE of the front, rear, and tandem solar cells. Figure 9b illustrates the absorbed spectrum of AM1.5G by the CPSC/CIGS-GeTe tandem solar cell. The cut-off wavelength of this cell is about 1558 nm,

according to the energy gap of the GeTe. As a result, the enhancement of the tandem solar cell is achieved.

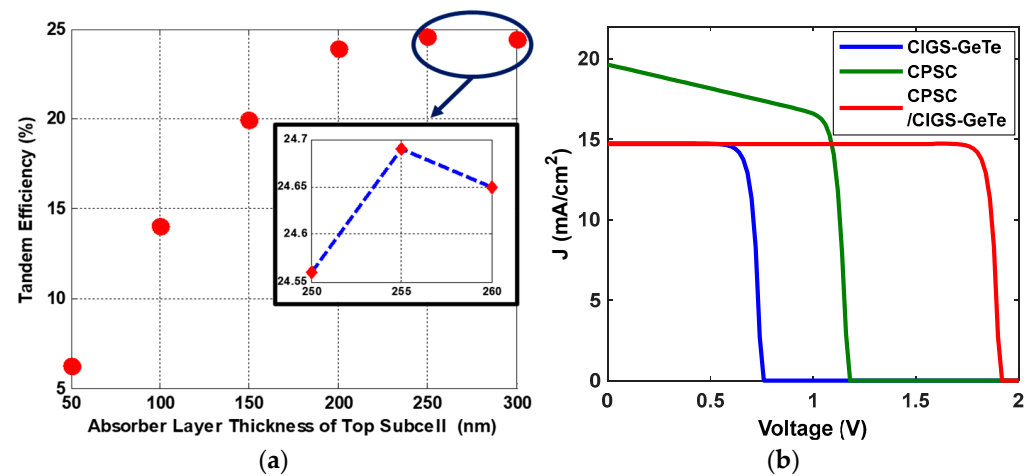


Figure 8. (a) PCE of CPSC/CIGS-GeTe tandem solar cell with the thickness of the top cell's absorber, and (b) JV curves of CPSC/CIGS-GeTe sub-cells besides the tandem solar cell.

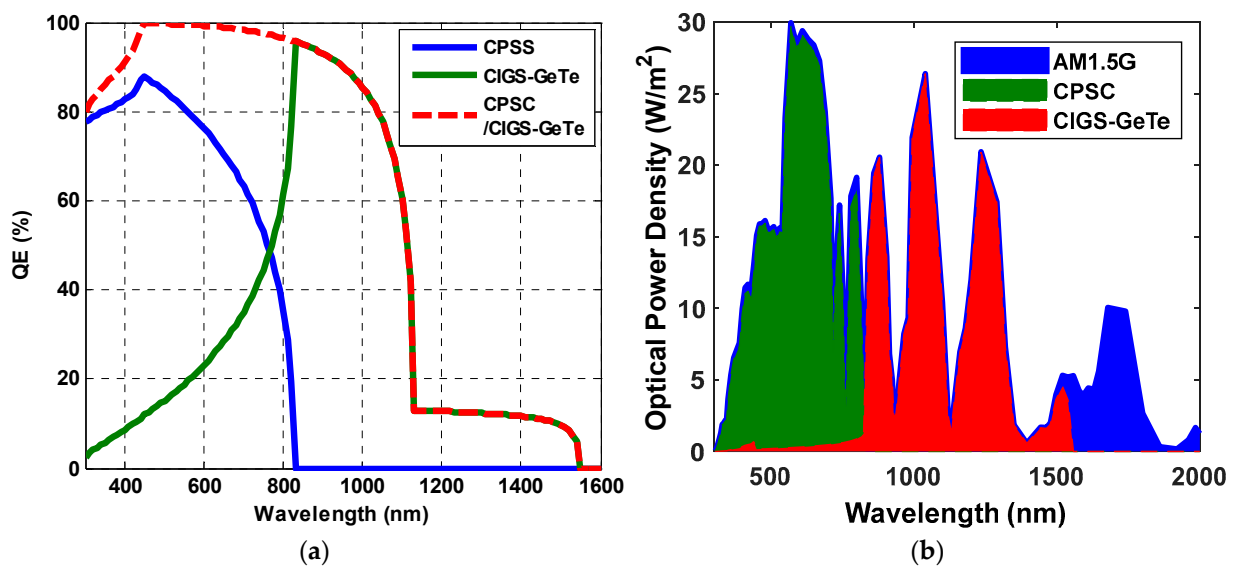


Figure 9. (a) EQE curves of CPSC/CIGS-GeTe sub-cells and tandem solar cell, and (b) the absorbed spectrum of AM1.5G by the CPSC/CIGS-GeTe tandem solar cell.

3.3. Temperature Impact on the Performance of CPSC Tandem Solar Cells

The carbon perovskite-based tandem solar cells show good stability and immunity to temperature change. Figure 10 illustrates the performance parameters of CPSC-based tandem solar cells under the variation of temperature. The PCE of tandem solar cells using CPSC as the top cell changes by less than 4% when the temperature is changed from 260 K to 360 K. It has been proven that the short circuit current density increases a bit when the temperature increases [65,66]. Testing the performance of the tandem solar cell with temperature variations shows the stability of the current density. In contrast, the variations of PCE and FF can be explained because of the voltage variation, which can be explained based on Equation (9).

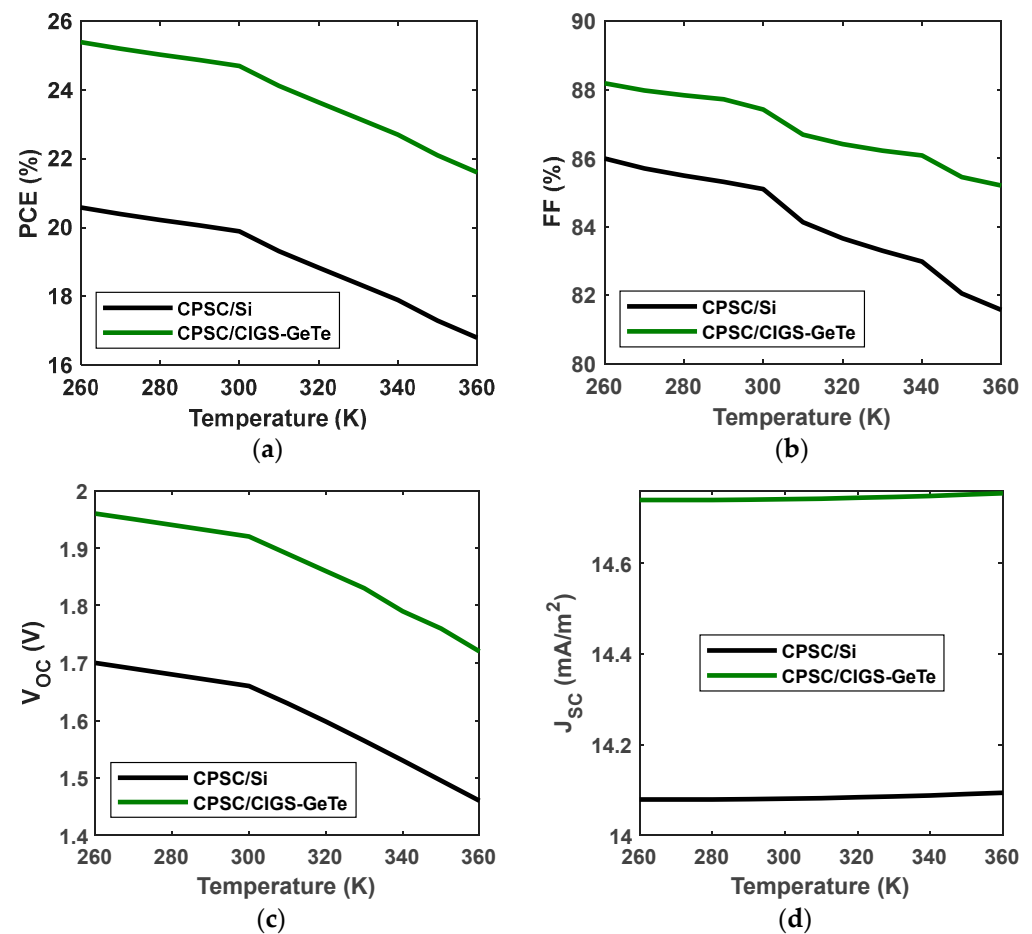


Figure 10. Performance parameters of CPSC-based tandem solar cells under the variation of temperature: (a) PCE, (b) FF, (c) V_{OC} , and (d) J_{SC} .

3.4. Comparison with the Recent Published Results

The PCE of some recent tandem solar cells during the past several years is described in this section. In this context, Table 4 compares the results of this study and other published results. In addition to the good stability behavior of the proposed tandem solar cells, they show comparative PCEs with state-of-the-art solar cells. It should be pointed out here that the utilized Si bottom cell, in our work, is a thin-film-based cell. On the other hand, the used bottom cell reported in [67] is Si wafer-based tandem in which the Si thickness is 280 μm . A thin film bottom cell is remarkably required for producing flexible solar cells under perovskite top cells.

Table 4. A comparison of the proposed tandem solar cells with the recently published data.

PCE (%)	The Material of Top/Bottom Sub Cells	Ref.-Year
19.89	CPSC/Si	This work
21.40	PSC/SHJ	[68]
22.50	PSC/Si	[67]
22.70	PSC/SHJ	[69]
23.26	PSC/CIGS	[70]
23.60	PSC/SHJ	[71]
23.60	PSC/SHJ	[71]
24.69	CPSC/CIGS-GeTe	This work
25.00	Four-terminals PSC/CIGS	[69]

4. Conclusions

Multi-junction solar cells have proven to be a better alternative than single-junction solar cells as it guarantees a higher PCE than single-junction cells. The ability of multi-junction solar cells to absorb a wide spectrum leads to better PCE which is improved as the number of junctions increases. However, increasing the number of junctions raises the cell's complexity and expense. CPSCs without HTL and with carbon as a back electrode stacked directly to the perovskite layer are introduced to enhance the stability of the top sub-cell. The simulation of CPSC started with the validation of the proposed cell with a practical published CPSC with a record PCE of 14.38%. CPSC with ZnSe as ETL shows the best performance when compared with other ETMs, including the traditional one, TiO₂. The main material parameters of the proposed ZnSe/CPSC are optimized to enhance performance. Splitting the absorber layer with an optimized doping gradient technique enhances the performance of the CPSC with a PCE of 22.22%. This work uses two-junction solar cells, which results in a higher PCE. This is accomplished first by increasing the bottom cell open circuit voltage based on using two different absorber layers and then by proposing a solution to one of the primary concerns with two-terminal tandem solar cells; the sub-cell with the lowest current (usually the rear cell) pushes the tandem solar cell to work at its current density. Using copper indium gallium selenide-germanium telluride as absorbers in the back cell allows the front cell and the tandem solar cell to work at a greater current density, resulting in an improvement of the overall tandem solar cell performance. The proposed two-terminal CPSC/Si and CPSC/CIGS-GeTe tandem solar cells have PCEs of 19.89%, and 24.69%, respectively. All the suggested cells have the benefit of just having two junctions, which reduces the complexity and cost of solar cells. The simulation results can provide design recommendations for possible tandem applications that are based on high-stability PSCs.

Author Contributions: Conceptualization, A.S. (Ahmed Shaker), M.M., M.M.S., M.A., R.I.M., D.S.L. and A.S. (Ahmed Saeed); methodology, A.S. (Ahmed Shaker), M.M., M.M.S., M.A., R.I.M., D.S.L. and A.S. (Ahmed Saeed); validation and formal analysis, M.M., M.M.S., M.A., A.S. (Ahmed Shaker), R.I.M., D.S.L. and A.S. (Ahmed Saeed); visualization, M.M. and M.M.S.; investigation, all authors; writing—original draft preparation, A.S. (Ahmed Shaker), M.M., M.M.S., M.A., R.I.M. and A.S. (Ahmed Saeed); writing—review and editing, all authors; supervision, A.S. (Ahmed Shaker), F.Z.A., A.Z., M.A., R.I.M. and D.S.L. All authors have read and agreed to the published version of the manuscript.

Funding: This research received no external funding.

Institutional Review Board Statement: Not applicable.

Informed Consent Statement: Not applicable.

Data Availability Statement: No new data were created or analyzed in this study. Data sharing does not apply to this article.

Conflicts of Interest: The authors declare no conflict of interest.

References

1. Zekry, A. A road map for transformation from conventional to photovoltaic energy generation and its challenges. *J. King Saud Univ. Eng. Sci.* **2020**, *32*, 407–410. [\[CrossRef\]](#)
2. Zekry, A.; Shaker, A.; Salem, M. Solar Cells and Arrays: Principles, Analysis, and Design. *Adv. Renew. Energ. Power Technol.* **2018**, *1*, 3–56. [\[CrossRef\]](#)
3. Gao, P.; Grätzel, M.; Nazeeruddin, M.K. Organohalide lead perovskites for photovoltaic applications. *Energy Environ. Sci.* **2014**, *7*, 2448–2463. [\[CrossRef\]](#)
4. Li, X.; Yang, J.; Jiang, Q.; Chu, W.; Zhang, D.; Zhou, Z.; Xin, J. Synergistic Effect to High-Performance Perovskite Solar Cells with Reduced Hysteresis and Improved Stability by the Introduction of Na-Treated TiO₂ and Spraying-Deposited CuI as Transport Layers. *ACS Appl. Mater. Interfaces* **2017**, *9*, 41354–41362. [\[CrossRef\]](#) [\[PubMed\]](#)
5. Green, M.A.; Ho-Baillie, A.; Snaith, H.J. The emergence of perovskite solar cells. *Nat. Photonics* **2014**, *8*, 506–514. [\[CrossRef\]](#)
6. Lee, Y.H.; Luo, J.; Son, M.-K.; Gao, P.; Cho, K.T.; Seo, J.; Zakeeruddin, S.M.; Grätzel, M.; Nazeeruddin, M.K. Enhanced Charge Collection with Passivation Layers in Perovskite Solar Cells. *Adv. Mater.* **2016**, *28*, 3966–3972. [\[CrossRef\]](#)

7. Kojima, A.; Teshima, K.; Shirai, Y.; Miyasaka, T. Organometal halide perovskites as visible-light sensitizers for photovoltaic cells. *J. Am. Chem. Soc.* **2009**, *131*, 6050–6051. [\[CrossRef\]](#)
8. Yang, W.S.; Park, B.-W.; Jung, E.H.; Jeon, N.J.; Kim, Y.C.; Lee, D.U.; Shin, S.S.; Seo, J.; Kim, E.K.; Noh, J.H.; et al. Iodide management in formamidinium-lead-halide-based perovskite layers for efficient solar cells. *Science* **2017**, *356*, 1376–1379. [\[CrossRef\]](#)
9. Salah, M.M.; Abouelatta, M.; Shaker, A.; Hassan, K.M.; Saeed, A. A comprehensive simulation study of hybrid halide perovskite solar cell with copper oxide as HTM. *Semicond. Sci. Technol.* **2019**, *34*, 115009. [\[CrossRef\]](#)
10. Mousa, M.; Salah, M.M.; Zekry, A.; Abouelatta, M.; Shaker, A.; Amer, F.Z.; Mubarak, R.I.; Saeed, A. Simulation of High open-circuit voltage Perovskite/CIGS-GeTe tandem cell. In Proceedings of the 2022 IEEE 49th Photovoltaics Specialists Conference (PVSC), Philadelphia, PA, USA, 5–10 June 2022; pp. 1230–1234. [\[CrossRef\]](#)
11. Xing, G.; Mathews, N.; Sun, S.; Lim, S.S.; Lam, Y.M.; Grätzel, M.; Mhaisalkar, S.; Sum, T.C. Long-range balanced electron-and hole-transport lengths in organic-inorganic CH₃NH₃PbI₃. *Science* **2013**, *342*, 344–347. [\[CrossRef\]](#)
12. Laban, W.A.; Etgar, L. Depleted hole conductor-free lead halide iodide heterojunction solar cells. *Energy Environ. Sci.* **2013**, *6*, 3249–3253. [\[CrossRef\]](#)
13. Etgar, L. Semiconductor Nanocrystals as Light Harvesters in Solar Cells. *Materials* **2013**, *6*, 445–459. [\[CrossRef\]](#) [\[PubMed\]](#)
14. Kuang, C.; Tang, G.; Jiu, T.; Yang, H.; Liu, H.; Li, B.; Luo, W.; Li, X.; Zhang, W.; Lu, F.; et al. Highly Efficient Electron Transport Obtained by Doping PCBM with Graphdiyne in Planar-Heterojunction Perovskite Solar Cells. *Nano Lett.* **2015**, *15*, 2756–2762. [\[CrossRef\]](#)
15. Xiao, J.; Shi, J.; Liu, H.; Xu, Y.; Lv, S.; Luo, Y.; Li, D.; Meng, Q.; Li, Y. Efficient CH₃NH₃PbI₃ Perovskite Solar Cells Based on Graphdiyne (GD)-Modified P3HT Hole-Transporting Material. *Adv. Energy Mater.* **2015**, *5*, 1401943. [\[CrossRef\]](#)
16. Ku, Z.; Rong, Y.; Xu, M.; Liu, T.; Han, H. Full Printable Processed Mesoscopic CH₃NH₃PbI₃/TiO₂ Heterojunction Solar Cells with Carbon Counter Electrode. *Sci. Rep.* **2013**, *3*, 3132. [\[CrossRef\]](#)
17. Mei, A.; Li, X.; Liu, L.; Ku, Z.; Liu, T.; Rong, Y.; Xu, M.; Hu, M.; Chen, J.; Yang, Y.; et al. A hole-conductor-free, fully printable mesoscopic perovskite solar cell with high stability. *Science* **2014**, *345*, 295–298. [\[CrossRef\]](#) [\[PubMed\]](#)
18. Chen, H.; Wei, Z.; He, H.; Zheng, X.; Wong, K.S.; Yang, S. Solvent Engineering Boosts the Efficiency of Paintable Carbon-Based Perovskite Solar Cells to Beyond 14%. *Adv. Energy Mater.* **2016**, *6*, 1502087. [\[CrossRef\]](#)
19. Meng, X.; Zhou, J.; Hou, J.; Tao, X.; Cheung, S.H.; So, S.K.; Yang, S. Versatility of Carbon Enables All Carbon Based Perovskite Solar Cells to Achieve High Efficiency and High Stability. *Adv. Mater.* **2018**, *30*, 1706975. [\[CrossRef\]](#)
20. Xiao, Y.; Wang, C.; Kondamareddy, K.K.; Liu, P.; Qi, F.; Zhang, H.; Guo, S.; Zhao, X.-Z. Enhancing the performance of hole-conductor free carbon-based perovskite solar cells through rutile-phase passivation of anatase TiO₂ scaffold. *J. Power Sources* **2019**, *422*, 138–144. [\[CrossRef\]](#)
21. Chen, R.; Feng, Y.; Zhang, C.; Wang, M.; Jing, L.; Ma, C.; Bian, J.; Shi, Y. Carbon-based HTL-free modular perovskite solar cells with improved contact at perovskite/carbon interfaces. *J. Mater. Chem. C Mater.* **2020**, *8*, 9262–9270. [\[CrossRef\]](#)
22. Mousa, M.; Amer, F.Z.; Mubarak, R.I.; Saeed, A. Simulation of Optimized High-Current Tandem Solar-Cells with Efficiency Beyond 41%. *IEEE Access* **2021**, *9*, 49724–49737. [\[CrossRef\]](#)
23. Shockley, W.; Queisser, H.J. Detailed Balance Limit of Efficiency of p-n Junction Solar Cells. *J. Appl. Phys.* **2004**, *32*, 510. [\[CrossRef\]](#)
24. De Vos, A. Detailed balance limit of the efficiency of tandem solar cells. *J. Phys. D. Appl. Phys.* **1980**, *13*, 839. [\[CrossRef\]](#)
25. Salah, M.M.; Zekry, A.; Shaker, A.; Abouelatta, M.; Mousa, M.; Saeed, A. Investigation of Electron Transport Material-Free Perovskite/CIGS Tandem Solar Cell. *Energies* **2022**, *15*, 6326. [\[CrossRef\]](#)
26. Abdelaziz, W.; Zekry, A.; Shaker, A.; Abouelatta, M. Numerical study of organic graded bulk heterojunction solar cell using SCAPS simulation. *Sol. Energy* **2020**, *211*, 375–382. [\[CrossRef\]](#)
27. Burgelman, M.; Decock, K.; Khelifi, S.; Abass, A. Advanced electrical simulation of thin film solar cells. *Thin Solid Film.* **2013**, *535*, 296–301. [\[CrossRef\]](#)
28. Haddout, A.; Raidou, A.; Fahoume, M. Influence of the layer parameters on the performance of the CdTe solar cells. *Optoelectron. Lett.* **2018**, *14*, 98–103. [\[CrossRef\]](#)
29. Ishikawa, R.; Watanabe, S.; Yamazaki, S.; Oya, T.; Tsuboi, N. Perovskite/graphene solar cells without a hole-transport layer. *ACS Appl. Energy Mater.* **2019**, *2*, 171–175. [\[CrossRef\]](#)
30. Basyoni, M.S.S.; Salah, M.M.; Mousa, M.; Shaker, A.; Zekry, A.; Abouelatta, M.; Alshammari, M.T.; Al-Dhlan, K.A.; Gontrand, C. On the Investigation of Interface Defects of Solar Cells: Lead-Based vs Lead-Free Perovskite. *IEEE Access* **2021**, *9*, 130221–130232. [\[CrossRef\]](#)
31. Scharfetter, D.L.; Gummel, H.K. Large-Signal Analysis of a Silicon Read Diode Oscillator. *IEEE Trans. Electron Devices* **1969**, *16*, 64–77. [\[CrossRef\]](#)
32. Gummel, H.K. A Self-Consistent Iterative Scheme for One-Dimensional Steady State Transistor Calculations. *IEEE Trans. Electron Devices* **1964**, *11*, 455–465. [\[CrossRef\]](#)
33. Boumaour, M.; Sali, S.; Kermadi, S.; Zougar, L.; Bahfir, A.; Chaieb, Z. High efficiency silicon solar cells with back ZnTe layer hosting IPV effect: A numerical case study. *J. Taibah Univ. Sci.* **2019**, *13*, 696–703. [\[CrossRef\]](#)
34. Kim, K.; Gwak, J.; Ahn, S.K.; Eo, Y.-J.; Park, J.H.; Cho, J.-S.; Kang, M.G.; Song, H.-E.; Yun, J.H. Simulations of chalcopyrite/c-Si tandem cells using SCAPS-1D. *Sol. Energy* **2017**, *145*, 52–58. [\[CrossRef\]](#)
35. Mandadapu, U.; Vedanayakam, S.V.; Thyagarajan, K. Simulation and Analysis of Lead based Perovskite Solar Cell using SCAPS-1D. *Indian J. Sci. Technol.* **2017**, *10*, 1–8. [\[CrossRef\]](#)
36. Burgelman, M.; Decock, K.; Niemegeers, A.; Verschraegen, J.; Degraeve, S. *SCAPS Manual*; University of Gent: Gent, Belgium, 2021.

37. Salah, M.M.; Hassan, K.M.; Abouelatta, M.; Shaker, A. A comparative study of different ETMs in perovskite solar cell with inorganic copper iodide as HTM. *Optik* **2019**, *178*, 958–963. [CrossRef]
38. Noman, M.A.A.; Abden, M.J.; Islam, M.A. Germanium Telluride Absorber Layer, A proposal for Low Illumination Photovoltaic Application Using AMPS 1D. In Proceedings of the International Conference on Computer, Communication, Chemical, Material and Electronic Engineering, IC4ME2 2018, Rajshahi, Bangladesh, 8–9 February 2018. [CrossRef]
39. Gloeckler, M. Device Physics of Cu(In,Ga)Se₂ Thin-Film Solar Cells . . . " 2015. Available online: <https://www.yumpu.com/en/document/view/50809695/device-physics-of-cuingase2-thin-film-solar-cells> (accessed on 18 September 2022).
40. Asaduzzaman, M.; Hasan, M.; Bahar, A.N. An investigation into the effects of band gap and doping concentration on Cu(In,Ga)Se₂ solar cell efficiency. *Springerplus* **2016**, *5*, 1–8. [CrossRef]
41. Xu, J.; Fang, M.; Chen, J.; Zhang, B.; Yao, J.; Dai, S. ZnO-Assisted Growth of CH₃NH₃PbI₃-xCl_x Film and Efficient Planar Perovskite Solar Cells with a TiO₂/ZnO/C60 Electron Transport Trilayer. *ACS Appl. Mater. Interfaces* **2018**, *10*, 20578–20590. [CrossRef]
42. Chae, J.; Dong, Q.; Huang, J.; Centrone, A. Chloride Incorporation Process in CH₃NH₃PbI_{3-x}Cl_x Perovskites via Nanoscale Bandgap Maps. *Nano Lett.* **2015**, *15*, 8114–8121. [CrossRef]
43. Abdelaziz, S.; Zekry, A.; Shaker, A.; Abouelatta, M. Investigating the performance of formamidinium tin-based perovskite solar cell by SCAPS device simulation. *Opt. Mater.* **2020**, *101*, 109738. [CrossRef]
44. Samiee, M.; Konduri, S.; Ganapathy, B.; Kottokkaran, R.; Abbas, H.A.; Kitahara, A.; Joshi, P.; Zhang, L.; Noack, M.; Dalal, V. Defect density and dielectric constant in perovskite solar cells. *Appl. Phys. Lett.* **2014**, *105*, 153502. [CrossRef]
45. Chandramohan, R.; Sanjeeviraja, C.; Mahalingam, T. Preparation of zinc selenide thin films by electrodeposition technique for solar cell applications. *Phys. Status Solidi A Appl Res.* **1997**, *163*, R11–R12.
46. Naval, V.; Smith, C.; Ryzhikov, V.; Naydenov, S.; Alves, F.; Karunasiri, G. Zinc Selenide-Based Schottky Barrier Detectors for Ultraviolet-A and Ultraviolet-B Detection. *Adv. Optoelectron.* **2010**, *2010*, 1–5. [CrossRef]
47. Mousa, M.; Salah, M.M.; Amer, F.Z.; Saeed, A.; Mubarak, R.I. High Efficiency Tandem Perovskite/CIGS Solar Cell. In Proceedings of the 2020 2nd International Conference on Smart Power and Internet Energy Systems, SPIES 2020, Bangkok, Thailand, 15–18 September 2020; pp. 224–227. [CrossRef]
48. Du, H.-J.; Wang, W.-C.; Gu, Y.-F. Simulation design of P–I–N-type all-perovskite solar cells with high efficiency. *Chin. Phys. B* **2017**, *26*, 028803. [CrossRef]
49. Karimi, E.; Ghorashi, S.M.B. Investigation of the influence of different hole-transporting materials on the performance of perovskite solar cells. *Optik* **2017**, *130*, 650–658. [CrossRef]
50. Adachi, S.; Taguchi, T. Optical properties of ZnSe. *Phys. Rev. B* **1991**, *43*, 9569. [CrossRef]
51. Bansal, S.; Aryal, P. Evaluation of new materials for electron and hole transport layers in perovskite-based solar cells through SCAPS-1D simulations. In Proceedings of the Conference Record of the IEEE Photovoltaic Specialists Conference, Portland, OR, USA, 5–10 June 2016; Volume 2016, pp. 747–750. [CrossRef]
52. Madelung, O. *Semiconductors: Data Handbook*; Springer: Berlin/Heidelberg, Germany, 2004. [CrossRef]
53. Hossain, M.I.; Alharbi, F.H.; Tabet, N. Copper oxide as inorganic hole transport material for lead halide perovskite based solar cells. *Sol. Energy* **2015**, *120*, 370–380. [CrossRef]
54. Tajima, S.; Itoh, T.; Hazama, H.; Ohishi, K.; Asahi, R. Improvement of the open-circuit voltage of Cu₂ZnSnS₄ solar cells using a two-layer structure. *Appl. Phys. Express* **2015**, *8*, 082302. [CrossRef]
55. Hao, L.; Zhang, M.; Ni, M.; Shen, X.; Feng, X. Simulation of a Silicon Heterojunction Solar Cell with a Gradient Doping Emitter Layer. *J. Electron. Mater.* **2019**, *48*, 4688–4696. [CrossRef]
56. Lin, L.; Li, P.; Jiang, L.; Kang, Z.; Yan, Q.; Xiong, H.; Lien, S.; Zhang, P.; Qiu, Y. Boosting efficiency up to 25% for HTL-free carbon-based perovskite solar cells by gradient doping using SCAPS simulation. *Sol. Energy* **2021**, *215*, 328–334. [CrossRef]
57. Hwang, I.; Jeong, Y.; Shiratori, Y.; Park, J.; Miyajima, S.; Yoon, I.; Seo, K. Effective Photon Management of Non-Surface-Textured Flexible Thin Crystalline Silicon Solar Cells. *Cell. Rep. Phys. Sci.* **2020**, *1*, 100242. [CrossRef]
58. Frohna, K.; Stranks, S.D. Hybrid Perovskites for Device Applications. In *Handbook of Organic Materials for Electronic and Photonic Devices*; Woodhead Publishing: Sawston, UK, 2019; pp. 211–256. [CrossRef]
59. Dziewior, J.; Schmid, W. Auger coefficients for highly doped and highly excited silicon. *Appl. Phys. Lett.* **2008**, *31*, 346. [CrossRef]
60. Del Alamo, J.A.; Swanson, R.M. The Physics and Modeling of Heavily Doped Emitters. *IEEE Trans. Electron. Devices* **1984**, *31*, 1878–1888. [CrossRef]
61. Fossum, J.G.; Mertens, R.P.; Lee, D.S.; Nijs, J.F. Carrier recombination and lifetime in highly doped silicon. *Solid State Electron.* **1983**, *26*, 569–576. [CrossRef]
62. Li, J.; Chen, Z.; Zhang, X.; Sun, Y.; Yang, J.; Pei, Y. Electronic origin of the high thermoelectric performance of GeTe among the p-type group IV monoteellurides. *NPG Asia Mater.* **2017**, *9*, e353. [CrossRef]
63. Yeboah, D.; Singh, J. Study of the Contributions of Donor and Acceptor Photoexcitations to Open Circuit Voltage in Bulk Heterojunction Organic Solar Cells. *Electronics* **2017**, *6*, 75. [CrossRef]
64. Bisquert, J. The Physics of Solar Cells: Organic-Inorganic Halide Perovskite Photovoltaics. 2018. Available online: https://books.google.com/books/about/The_Physics_of_Solar_Cells.html?id=qXFQDwAAQBAJ (accessed on 12 December 2022).
65. Singh, P.; Ravindra, N.M. Temperature dependence of solar cell performance—An analysis. *Sol. Energy Mater. Sol. Cells* **2012**, *101*, 36–45. [CrossRef]
66. Wysocki, J.J.; Rappaport, P. Effect of Temperature on Photovoltaic Solar Energy Conversion. *J. Appl. Phys.* **2004**, *31*, 571. [CrossRef]

67. Sahli, F.; Kamino, B.A.; Werner, J.; Bräuninger, M.; Paviet-Salomon, B.; Barraud, L.; Monnard, R.; Seif, J.P.; Tomasi, A.; Jeangros, Q.; et al. Improved Optics in Monolithic Perovskite/Silicon Tandem Solar Cells with a Nanocrystalline Silicon Recombination Junction. *Adv. Energy Mater.* **2018**, *8*, 1701609. [[CrossRef](#)]
68. Werner, J.; Weng, C.H.; Walter, A.; Fesquet, L.; Seif, J.P.; De Wolf, S.; Niesen, B.; Ballif, C. Efficient Monolithic Perovskite/Silicon Tandem Solar Cell with Cell Area >1 cm². *J. Phys. Chem. Lett.* **2016**, *7*, 161–166. [[CrossRef](#)]
69. Gharibzadeh, S.; Hossain, I.M.; Fassel, P.; Nejand, B.A.; Abzieher, T.; Schultes, M.; Ahlswede, E.; Jackson, P.; Powalla, M.; Schäfer, S.; et al. 2D/3D Heterostructure for Semitransparent Perovskite Solar Cells with Engineered Bandgap Enables Efficiencies Exceeding 25% in Four-Terminal Tandems with Silicon and CIGS. *Adv. Funct. Mater.* **2020**, *30*, 1909919. [[CrossRef](#)]
70. Hutchins, M. HZB Hits 23.26% Efficiency with CIGS-Perovskite Tandem Cell. 2019. Available online: <https://www.pv-magazine.com/2019/09/11/hzb-hits-23-26-efficiency-with-cigs-perovskite-tandem-cell/> (accessed on 19 January 2023).
71. Bush, K.A.; Manzoor, S.; Frohna, K.; Yu, Z.J.; Raiford, J.A.; Palmstrom, A.F.; Wang, H.-P.; Prasanna, R.; Bent, S.F.; Holman, Z.C.; et al. Minimizing Current and Voltage Losses to Reach 25% Efficient Monolithic Two-Terminal Perovskite-Silicon Tandem Solar Cells. *ACS Energy Lett.* **2018**, *3*, 2173–2180. [[CrossRef](#)]

Disclaimer/Publisher’s Note: The statements, opinions and data contained in all publications are solely those of the individual author(s) and contributor(s) and not of MDPI and/or the editor(s). MDPI and/or the editor(s) disclaim responsibility for any injury to people or property resulting from any ideas, methods, instructions or products referred to in the content.